Double photoionization of helium at an excess energy of 60 eV using left- and right-elliptically-polarized light

S. A. Collins,[1] S. Cvejanović,[1,*] C. Dawson,[1] T. J. Reddish,[1] D. P. Seccombe,[1] A. Huetz,[2] L. Malegat,[2] P. Selles,[2] A. K. Kazansky,[3] A. Danjo,[4] K. Soejima,[4] K. Okuno,[5] and A. Yagishita[6]

[1]*Physics Department, Newcastle University, Newcastle upon Tyne, NE1 7RU, United Kingdom*

[2]*Laboratoire de Spectroscopie Atomique et Ionique (UMR 8624 du CNRS), Université Paris–Sud, Bâtiment 350, 91405 Orsay Cedex, France*

[3]*Fock Institute of Physics, The University of St. Petersburg, St. Petersburg 198504, Russia*

[4]*Graduate School of Science and Technology, Niigata University, Niigata-shi 950-21, Japan*

[5]*Department of Physics, Tokyo Metropolitan University, Hachioji-shi, Tokyo 192-03, Japan*

[6]*Photon Factory, Institute of Materials Structure Science, KEK, Tsukuba-shi 305, Japan*

(Received 27 December 2001; published 6 May 2002)

Helium double photoionization $(\gamma,2e)$ triple differential cross sections (TDCSs) were measured at an excess energy of 60 eV using a dual toroidal spectrometer and synchrotron radiation from a helical undulator (BL-28A, Photon Factory, Japan). Energy-sharing ratios $(R=E_2/E_1)$ for the two ejected electrons of 5 and 11 are studied with both right- and left-handed elliptically polarized light. The TDCSs are found to be in good agreement with those obtained using the hyperspherical $\mathcal{R}$ matrix with semiclassical outgoing waves theory. The circular dichroism for a limited mutual angular range $(\phi_{12}\approx 110°-200°)$ is determined from the experimental data for both $R=5$ and 11, and compared to theoretical calculations performed over the complete range of mutual angles. No dynamic nodes are found in either the experimental (within the explored ϕ_{12} range) or theoretical circular dichroism for these R values at this excess energy.

DOI: 10.1103/PhysRevA.65.052717 PACS number(s): 32.80.Fb

I. INTRODUCTION

Double photoionization (DPI) (the absorption of a single photon followed by the emission of two electrons $[\gamma,2e]$) in helium has been the subject of a large number of experimental and theoretical investigations over the last decade (for a recent review of the field, see [1]). Since this process produces two free electrons and a bare nucleus, it presents an ideal opportunity to probe the dynamics of three bodies interacting via the long-range Coulomb force. Experimentally, there have been numerous measurements of $(\gamma,2e)$ triple differential cross sections (TDCSs) using radiation with essentially zero circular polarization contribution (i.e., Stokes parameter $S_3=0$) [2–19]. If the energy in excess of the double ionization threshold (79.0 eV) is denoted by E, and the energies of the two electrons by E_1 and E_2, then TDCSs have been reported from $E=0.1$ eV [15] up to $E=80$ eV [19] for a variety of energy-sharing ratios $(R=E_2/E_1)$. The experiments have generally yielded relative TDCSs, where the overall shapes of the distributions with respect to the mutual angle ϕ_{12} are measured without any absolute scale. Those groups who have measured absolute cross sections have achieved this using 4π detection [11,13,15], with the exception of Schwarzkopf and Schmidt [8], who made absolute cross-section measurements with two cylindrical mirror analyzers. All these experiments have required an external reference (such as the total single photoionization cross section, σ^+) to put the data on an absolute scale. Theoretically, various methods have emerged to deal with DPI of He or the related process of electron-impact ionization of H [20–30]. Recent calculations have utilized the converged close coupling (CCC) [23,24], the exterior complex scaling (ECS) [25], the time-dependent close coupling (TDCC) [26,27], and the hyperspherical $\mathcal{R}$ matrix with semiclassical outgoing waves (H$\mathcal{R}$M-SOW) [28–30] techniques. In the case of linearly polarized light there is now good agreement between experiment and theory for most values of E and R as far as the shapes of the TDCSs are concerned. Achieving agreement on the absolute scale has proved more difficult: for examples of agreement with absolute measurements see Refs. [27,30].

Significant progress in understanding the structure of the TDCS was made by Huetz *et al.* [31] who succeeded in identifying its geometrical and dynamic constituents. The geometrical factors arise simply from the symmetry of the initial state, the optical selection rules, and the polarization state of the synchrotron radiation. Huetz and co-workers [31,6] showed that the dynamics of the process are completely described by two complex amplitudes $a_g(E,R,\phi_{12})$ and $a_u(E,R,\phi_{12})$, which are, respectively, symmetric and antisymmetric with respect to interchange of the electrons' energy. Extracting information pertaining to these fundamental quantities from the measured cross sections is a current challenge. The direct extraction of these amplitudes has been achieved in a few cases [2,32,33], but most attempts have relied upon parametrizations of a_g and a_u with various degrees of complexity. A universal parametrization of the angular dependence of a_g and a_u has been derived by Malegat, Selles, and Huetz [34] and applied to experimental data [35,36]. The use of this parametrization has been restricted

*Present address: Fritz-Haber-Institut der Max-Planck-Gesellschaft, Faradayweg 4-6, D-14195, Berlin, Germany.

because of the relatively large number of fitting parameters required. The simpler, ''practical'' parametrization of Cvejanović and Reddish [37] has been used to fit experimental TDCSs [37,17] and those determined using the CCC theory [38]. The CCC method has also been used to investigate the a_g and a_u amplitudes that underlie the TDCS [38], which, together with future publications of those obtained using H$\mathcal{R}$M-SOW or TDCC theories, will help assess the limits of validity of this intuitive parametrization.

The search for information on these ''building blocks'' of the DPI cross section has stimulated fresh experimental approaches. The recording of pairs of TDCSs having complementary electron energy ratios R and R^{-1} using linearly polarized light has given access to their difference [6,17], which is proportional to the cosine of the phase difference χ $(=\delta_u-\delta_g)$ between a_g and a_u. Alternatively, the measurement of pairs of TDCSs obtained using left- and right-circularly-polarized light, respectively, allows one to obtain their difference, referred to as the circular dichroism (CD), proportional to the sine of χ.

Circular dichroism in the helium double photoionization TDCS was first predicted by Berakdar and Klar [39]. They showed that, if the discussion is restricted to the double photoionization of ground-state helium, then circular dichroism should be observed for $R\neq 1$ provided the electron emission directions $(\vec{k}_1,\vec{k}_2)$ and the photon propagation direction $\vec{k}_\gamma$ are not coplanar. The work of Berakdar and Klar [39] has been followed by other theoretical studies that extend and quantify the effect [24,40–43]. The whole issue of chirality in multielectron emission is discussed in two recent review articles [44].

Experimentally, circular dichroism in the helium $(\gamma,2e)$ TDCS was first observed by Viefhaus *et al.* [45], who, using electron time-of-flight spectroscopy, observed the effect for three mutual angles ($\phi_{12}=85°$, 125°, and 150°) and five energy ratios $(R=0.1,0.3,0.5,0.7,0.9)$. This study, utilizing linearly polarized radiation $(h\nu=93.5\ \text{eV}, E=14.5\ \text{eV})$ from BESSYI incident upon a quarter wave plate, has been followed by several more comprehensive experiments using right- and left-elliptically-polarized light from a helical undulator (BL-28A) at the Photon Factory [36,43,46,47]. ''Cold target recoil ion momentum spectroscopy'' has been used to measure absolute TDCSs and obtain the circular dichroism at 20 eV above threshold for a variety of energy-sharing ratios [46,47]. Soejima *et al.* [36] using two parallel-plate analyzers measured relative TDCSs in the perpendicular plane for $E=9$ eV and $R=8$. They investigated a_g and a_u using parametrization methods to deduce the linear and circular contributions to the TDCS. In a later publication their TDCSs were found to be consistent with those obtained using the CCC theory [43]. The kinematic conditions investigated in all these experimental studies are summarized in Table I.

In contrast to previous work, the present study employs an excess energy of 60 eV $(h\nu=139\ \text{eV})$, which is above the peak in the total DPI cross section at $E\sim 23$ eV $(h\nu=102$ eV) (Ref. [48] and references therein). Nonabsolute TDCSs for $R=5$ and 11 were measured over a wide range of angles using a dual toroidal electron spectrometer. The TDCSs and the circular dichroism obtained from them are compared with the results of the H$\mathcal{R}$M-SOW theory. The circular dichroism is also compared with that measured by Achler *et al.* [47] at the lower excess energy and interesting differences are found, which we believe relate to the different E and R values.

TABLE I. A summary of the previous experimental measurements of helium $(\gamma, 2e)$ triple differential cross sections, which have utilized elliptically polarized radiation.

Excess energy (E) (eV)	Energy ratio (R)	Study
14.5	0.1, 0.3, 0.5, 0.7, 0.9	Viefhaus *et al.* [45]
20	0.026, 0.08, 0.14, 0.38, 0.6	Mergel *et al.* [46][a]
9	8, 1	Soejima *et al.* [36]
9	8, 2, 1	Kheifets *et al.* [43]
20	0.026, 0.14, 0.38, 1	Achler *et al.* [47][a,b]

[a]Absolute measurements.

[b]Note that the data of Achler *et al.* [47] supersedes the previous work of Mergel *et al.* [46].

II. EXPERIMENTAL

The measurements were performed on the helical undulator beam line BL-28A [49–51] at the Photon Factory in Tsukuba, Japan. The beam line is equipped with a constant deviation monochromator and provides high-flux elliptically-polarized VUV radiation. The helical undulator operates in two elliptically-polarized modes, known as ''HUN'' and ''HUP,'' and a linearly polarized mode, ''LIN.''

Figure 1 illustrates these three modes and is plotted in the plane perpendicular to the photon beam, the direction of which is taken as the Z axis. Different right-handed frames are introduced within this plane: (i) the laboratory frame XOY with OX in the horizontal plane and (ii) the relative frame xOy, with Ox along the main axis of the polarization ellipse. xOy is rotated from XOY by an angle λ counterclockwise in the HUN mode and clockwise in the HUP mode. In the LIN mode, which is described in XOY by the Stokes parameters $S_1=0.99$, $S_2=0$, $S_3=0$, the electric field oscillates along OX. In the HUN mode, characterized in its relative frame xOy by the Stokes parameters $S_1=0.28\pm 0.03$, $S_2=0$, $S_3=-0.95\pm 0.02$, the electric field describes the ellipse in the counterclockwise direction. This mode corresponds to left-circular polarization in optics, or positive helicity and a positive projection of the angular momentum on the quantization axis in atomic physics [1]. In the HUP mode, characterized in its relative frame xOy by the Stokes parameters $S_1=0.28\pm 0.03$, $S_2=0$, $S_3=0.95\pm 0.02$, the electric field describes the ellipse in the clockwise direction. This mode corresponds to right-circular polarization, that is to say, negative helicity and a negative projection of the angular momentum on the quantization axis.

As the data analysis requires accurate knowledge of the Stokes parameters S_1 and S_3, it is worth noting the origin of the above-quoted values and those of the tilt angles λ that

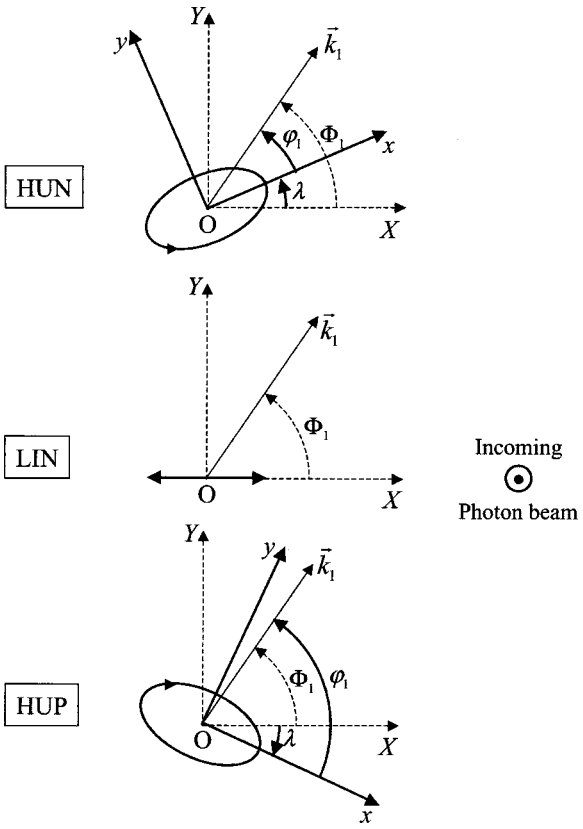

FIG. 1. Definition of the laboratory frame *XOY* and of the ±λ rotated frames *xOy* associated with the HUN and HUP modes, together with the angles Φ_i and φ_i corresponding to the $\vec{k}_i$ emission direction of each of the two electrons ($i=1,2$) in these different frames. The *Z* and *z* axes are both along the direction of the incoming photon beam, perpendicular to the plane of the figure (see text).

define the frames where $S_2=0$. The values related to the LIN mode are well-known characteristics of the BL-28A line. For the HUN and HUP modes, where the residual S_1 contribution is not negligible, it is desirable to determine these values under the actual experimental conditions. Unfortunately, S_3 could not be determined experimentally at this photon energy of 139 eV without an appropriate polarimeter, thus we quote the values measured at 97 eV by Kimura *et al.* [52]. A similar approach was adopted by Soejima *et al.* [36], based on the theoretical argument that the degree of circular polarization at the first harmonic is independent of the undulator gap [51] that determines its energy position. The value of S_1 was determined from our measurements of the He^+ ($n=1,2$) photoelectron angular distributions, both of which are characterized by well-known β values, obtained using the HUP and LIN modes. The ratio of the two He^+ ($n=2$) distributions, which, incidentally, eliminates variations in angular efficiency of the toroidal analyzers, was also used to estimate the HUP tilt angle (λ). The λ value obtained by this method was found to lie in the 30°–35° range. The tilt angles were also measured independently using an existing polarimeter and were found to be $30°\pm5°$ and $-30°\pm5°$ from the horizontal, for the HUN and HUP modes, respectively. We note, however, that these tilt angle values are significantly smaller than those obtained by Kimura *et al.* [52], namely, $\approx\pm45°$,

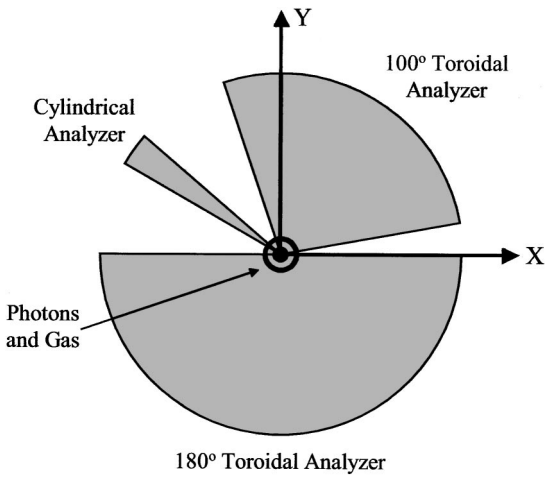

FIG. 2. Orientation of the three analyzers in the laboratory frame *XOY*. The *Z* axis, taken along the incoming photon beam, is perpendicular to the plane of the figure.

which were used in the analyses of [36,43,46,47].

The apparatus employed was the toroidal coincidence photoelectron spectrometer that has been described in detail elsewhere [53]. Briefly, the spectrometer consists of two partial toroidal analyzers with mechanical angular ranges of 100° and 180° and a cylindrical analyzer, which detect electrons emitted in the plane perpendicular to the photon beam (Fig. 2). Due to geometrical constraints and electric-field termination effects, the useful angular ranges of the small and large toroidal analyzers are limited to ~60° and ~140°, respectively. As in Dawson *et al.* [18], gas enters the vacuum chamber via a cylindrically symmetric nozzle, based on the design of Kämmerling and Schmidt [54], which is coaxial to the photon beam. This conical gas ''jet'' was developed to allow the cylindrical analyzer to be placed in the space previously occupied by a hypodermic needle.

Electron-electron coincidence measurements were made both between the small 100° (60°) and large 180° (140°) toroidal analyzers, and between the cylindrical and large toroidal analyzers. The energy-dependent angular responses of the toroidal analyzers were calibrated for each different photoelectron energy using the β values associated with the $He\rightarrow He^+$ $n=2$ transition. The β values that were used ($\beta=0.30$, 0.57, 1.48, and 1.53 for 5, 10, 50, and 55 eV, respectively) were obtained from a fit to the measurements of Wehlitz *et al.* [55]. It should be noted that the calibration assumes that the coincidence overlap is the same for each mutual angle. The full width at half maximum energy resolutions ΔE_{FWHM} for the two toroidal analyzers were chosen to be ~600 meV for electrons with energies ⩾30 eV and ~300 meV for electrons with energies <30 eV. The cylindrical analyzer was only used to detect electrons of energies ⩽30 eV and had an energy resolution of ~450 meV.

III. THEORY

The principles of the H$\mathcal{R}$M-SOW method and a limited selection of representative results were first given in [29]. The details of its implementation and a wide sample of cal-

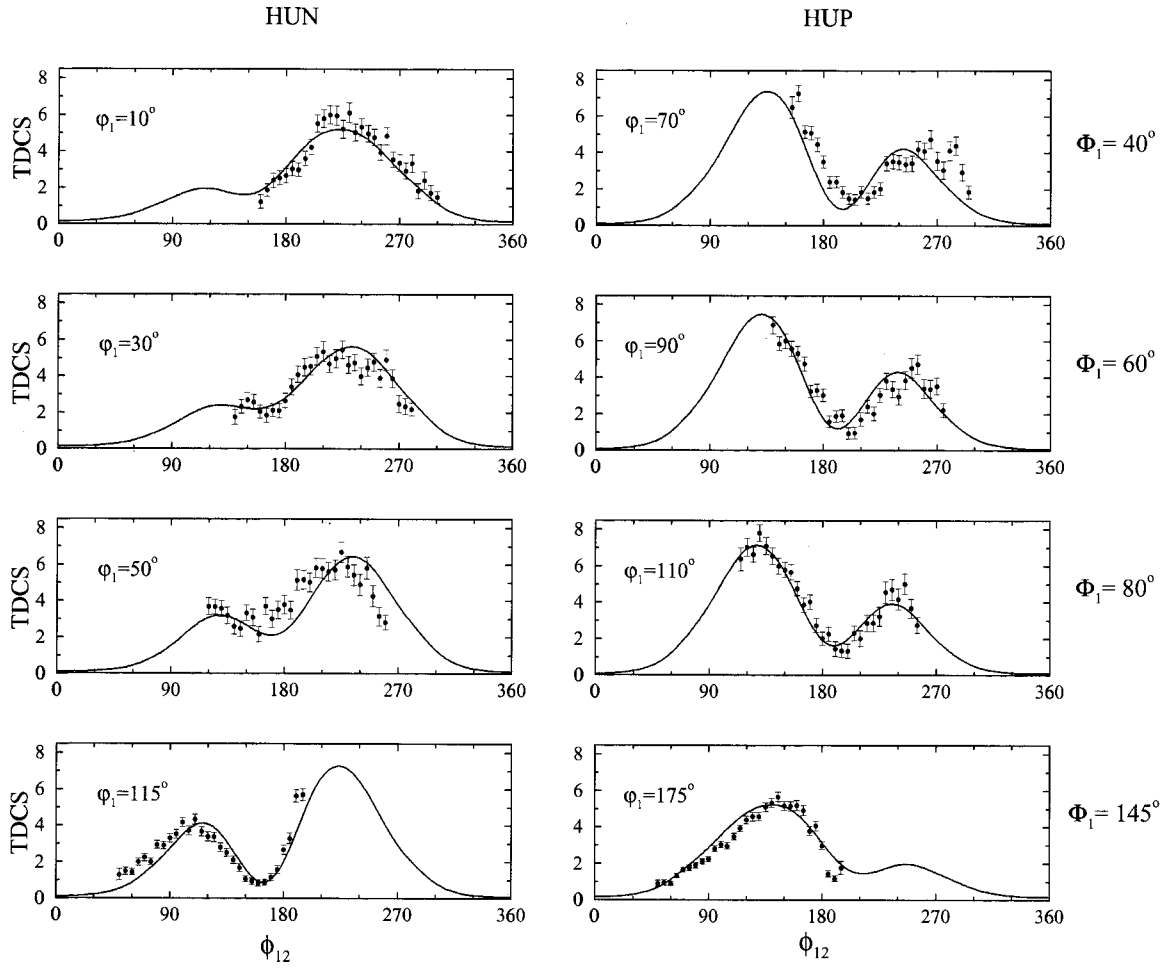

FIG. 3. TDCS ($\sigma^{(3)}$) in b eV^{-1} sr^{-2} versus the mutual angle ϕ_{12} in degrees for $R=5$. The left column corresponds to the HUN mode, the right one to the HUP mode, as indicated in the figure. The different rows correspond to the various emission directions of the low-energy electron: from top to bottom, $\Phi_1=40°$, 60°, 80°, and 145° as indicated in the figure and discussed in the text. The corresponding φ_1 angles are contained within each plot.

culated single-, double-, and triple-differential cross sections can be found in [30]. Consequently, only a brief outline of the theory will be presented here.

The He DPI problem is formulated starting from the time-dependent Schrödinger equation. In contrast to the TDCC method [26,27], we do not attempt to solve this equation directly. Instead, we look for a solution in the form of a superposition of the initial state $\Psi_0(\vec{r}_1,\vec{r}_2)$ of energy E_0 and the state $\Psi_1(\vec{r}_1,\vec{r}_2)$ reached after absorption of one photon, each term being weighted by the appropriate time-oscillating phase factor. The stationary wave function $\Psi_1(\vec{r}_1,\vec{r}_2)$, which contains all information related to the final state in the double continuum, can then be obtained by solving the inhomogeneous equation

$$[H_0-(E_0+\omega)]\Psi_1(\vec{r}_1,\vec{r}_2)=-\tfrac{1}{2}\mathbf{E}_0\cdot\mathbf{D}\Psi_0(\vec{r}_1,\vec{r}_2) \quad (1)$$

satisfying the outgoing waves boundary conditions. In Eq. (1), H_0 denotes the field-free Hamiltonian, $\mathbf{E}_0$ the amplitude of the radiation field, and $\mathbf{D}$ the dipole operator. It is worth noting that there is a formal similarity between the present H$\mathcal{R}$M-SOW formulation of the DPI problem for He and the ECS formulation of the related electron-impact ionization problem for H [25].

Our procedure relies upon two main elements. First, the use of hyperspherical coordinates including the hyperspherical radius ρ, the radial correlation angle α, and a set of four angles specifying the directions of the two outgoing electrons. Second, the splitting of configuration space into two regions: an inner region $\rho\leqslant\rho_0$, where a full quantum $\mathcal{R}$-matrix approach is employed, and a complementary outer region, where a quantum treatment of all angular variables is combined with a semiclassical treatment of the variable ρ. The calculation then proceeds in three steps: first, the wave function on the hypersphere $\rho=\rho_0$ is extracted; second, it is propagated from ρ_0 to ρ_∞; third, the cross sections are extracted by computing the outgoing flux through the hypersphere $\rho=\rho_\infty$.

The original combination of $\mathcal{R}$-matrix and semiclassical techniques, which is at the heart of this method, allows one to respect the three-body nature of the system throughout configuration space and is the key to a reliable treatment of this long-standing problem. Low computational requirements

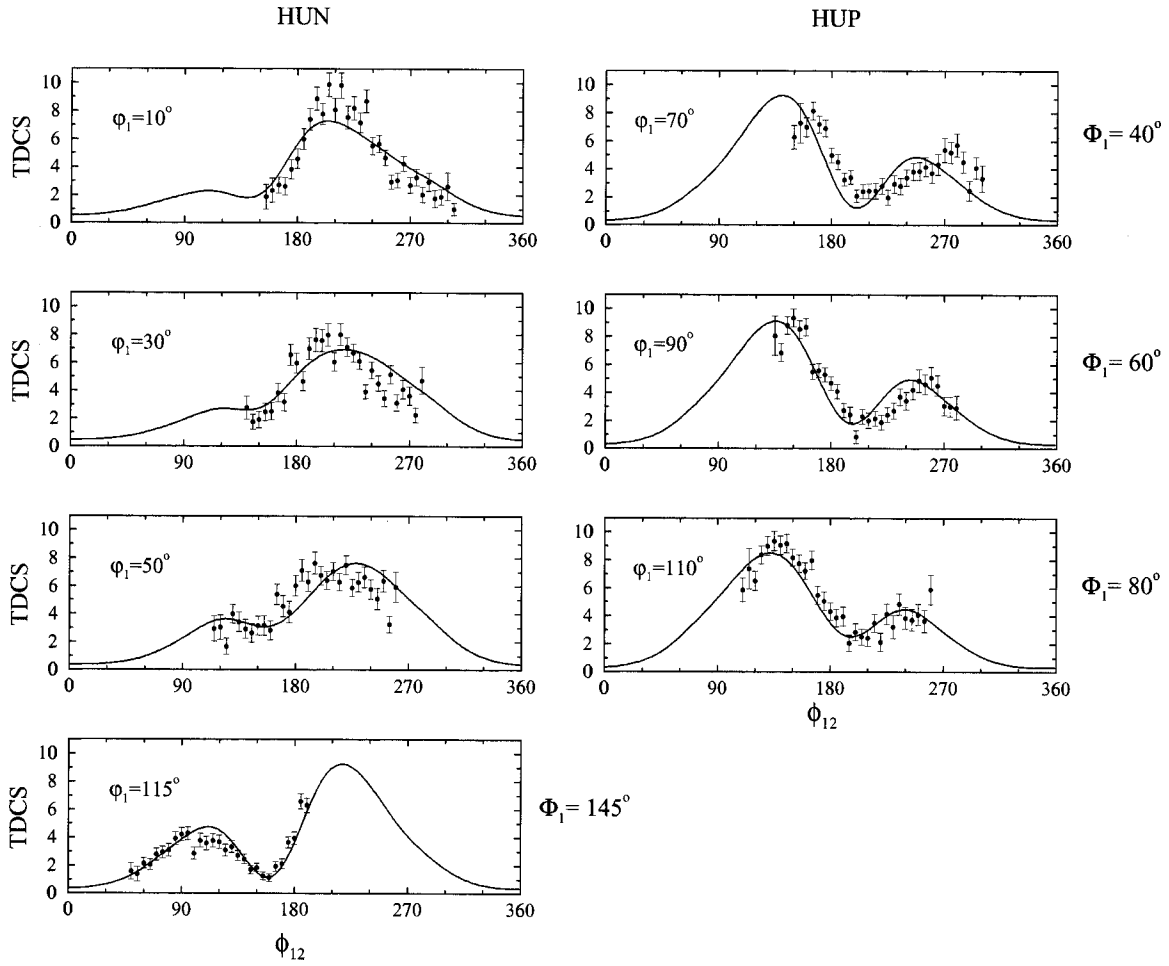

FIG. 4. Same as Fig. 3 but for $R=11$.

and the opportunity to witness the formation of the cross sections during the expansion of the system from $\rho=\rho_0=10$ a.u. to $\rho=\rho_\infty=10^5$ a.u. are subsidiary advantages of this approach.

All TDCSs computed so far using the H$\mathcal{R}$M-SOW method corresponded to DPI by linearly polarized radiation. The calculations reported here represent the application of H$\mathcal{R}$M-SOW to DPI using elliptically-polarized light.

IV. RESULTS AND DISCUSSION

A. Triple differential cross sections

As explained in Sec. II, the electrons are detected in the plane perpendicular to the direction of the photon (see Fig. 2), and the directions of their momenta $\vec{k}_{1,2}$ are characterized by the azimuthal angles $\Phi_{1,2}$, measured counterclockwise from *OX* in the laboratory frame, or alternatively by the azimuthal angles $\varphi_{1,2}$, measured counterclockwise from *Ox* in the rotated frames associated with each undulator mode (see Fig. 1). In order to minimize potential systematic errors caused by rotating the apparatus, the physical orientation of the spectrometer in the laboratory frame has been kept fixed at the position depicted by Fig. 2 in all undulator modes. The electron labeled 2 (in this experiment the faster one) is detected by the large toroidal analyzer over its useful angular range ($200°<\Phi_2<340°$), which is subdivided into 10°-wide sectors. This electron is detected in coincidence with that labeled 1 (the slower one in this work) at $\Phi_1=145°$, using the cylindrical analyzer, and over 20°-wide sectors centered at $\Phi_1=40°$, 60°, and 80° using the small toroidal analyser. These measurements have been performed for the two modes HUN and HUP and for the two energy ratios $R=5$ and $R=11$ at the fixed excess energy of 60 eV. The resulting TDCSs, plotted as a function of the mutual angle ϕ_{12}, are shown in Figs. 3 ($R=5$) and 4 ($R=11$). The full curves are the result of H$\mathcal{R}$M-SOW calculations and the agreement between experiment and theory is good. The non-absolute experimental TDCSs are normalized to the absolute values produced using the theory. In each mode the *same normalization constant* was applied to the three experimental TDCSs obtained from coincidence measurements involving the two toroidal analyzers.

One disadvantage of the present ''fixed spectrometer'' approach is that the range of ϕ_{12} investigated varies with Φ_1. The mutual angle ranges of the measured TDCSs are 160°–300°, 140°–280°, 120°–260°, and 50°–190° for $\Phi_1=40°$, 60°, 80°, and 145°, respectively. Accordingly, depending on Φ_1, the experimental points are centered on the main lobe, or on the secondary lobe, or in between the two lobes that are observed in the TDCSs, as one can see from Figs. 3 and 4. In

these circumstances, the computed curves prove particularly useful to make the general trends in the evolution of the angular patterns appear more clearly. These trends can be understood qualitatively from the expressions of the cross sections in terms of the amplitudes a_g and a_u and of the geometrical factors relative to the rotated frame associated with each mode. To establish these expressions, we begin from the general equation for the TDCS ($\sigma^{(3)}$) in terms of the Stokes parameters (see, for instance, [1,56])

$$\sigma^{(3)}=\frac{1}{2}(\sigma_x^{(3)}+\sigma_y^{(3)})+\frac{S_1}{2}(\sigma_x^{(3)}-\sigma_y^{(3)})+\frac{S_3}{2}(\sigma_R^{(3)}-\sigma_L^{(3)}), \tag{2}$$

where the contributions $\sigma_x^{(3)}$ and $\sigma_y^{(3)}$ arise from pure linear polarization along *Ox* and *Oy*, and the contributions $\sigma_R^{(3)}$ and $\sigma_L^{(3)}$ from pure right- and left-circular polarization, respectively. Note that $[S_3=0,\ S_1=1\ (-1)]$ corresponds to pure linear polarization along *Ox* (*Oy*) and $[S_1=0,\ S_3=1\ (-1)]$ to pure right- (left-) circular polarization, and the unpolarized contribution $\sigma_x^{(3)}+\sigma_y^{(3)}$ can also be written as $\sigma_R^{(3)}+\sigma_L^{(3)}$. The three terms in the TDCS can be expressed explicitly as functions of the complex amplitudes and the relevant geometrical factors to yield, in this perpendicular detection plane,

$$\begin{aligned}\sigma^{(3)}=&\{|a_g|^2(1+\cos\phi_{12})+|a_u|^2(1-\cos\phi_{12})\}\\&+S_1\{\cos(2\varphi_1+\phi_{12})[|a_g|^2(1+\cos\phi_{12})-|a_u|^2(1\\&-\cos\phi_{12})]-2\sin(2\varphi_1+\phi_{12})\sin\phi_{12}\,\mathrm{Re}(a_g a_u^*)\}\\&-2S_3\sin\phi_{12}\,\mathrm{Im}(a_g a_u^*),\end{aligned} \tag{3}$$

where the mutual angle is defined as $\phi_{12}=\varphi_2-\varphi_1$. One important feature of Eq. (3) concerning its angular dependencies is that the first and last terms depend only on the mutual angle ϕ_{12} while the second term, proportional to S_1, depends also on φ_1. If this second term were negligible, then the angular patterns would not change in any given column of Fig. 3 or 4, as a function of $\Phi_1(\varphi_1)$ for a given R value. The inspection of Figs. 3 and 4 shows that this second term is weak, as it does not change the general two-lobe structure of the TDCSs, it neither moves significantly the peak positions of the lobes nor inverses the ratio of their heights. It is nonnegligible, however, because it is able to alter this ratio significantly. This conclusion is consistent with the value of S_1 being much less than that of S_3. When one moves from the left to the right column in Fig. 3 or 4, thus switching from the HUN to the HUP mode, the main effect is the inversion of the ratio of the two peaks. This inversion is attributed to the change of sign of S_3. Namely, as the second term in Eq. (3) is weak, the main difference between the TDCSs recorded in the HUN and HUP modes arises from the third term.

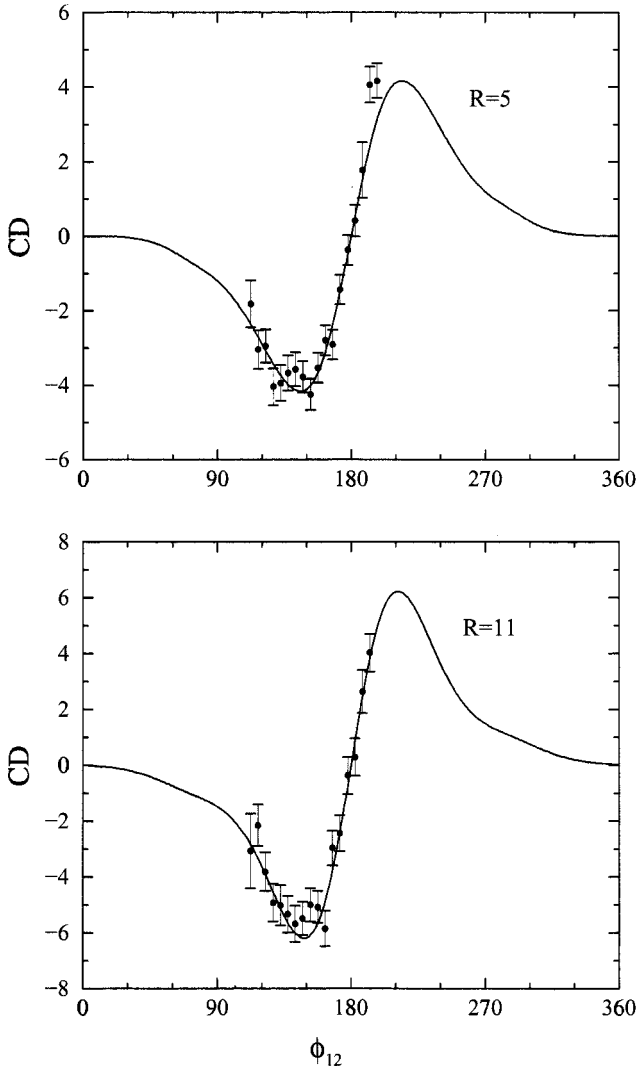

FIG. 5. CD in b $\mathrm{eV}^{-1}\,\mathrm{sr}^{-2}$ versus the mutual angle ϕ_{12} in degrees for $R=5$ (top pattern) and $R=11$ (bottom pattern).

B. Circular dichroism

The CD was defined in the Introduction as $(\mathrm{CD})=\sigma_L^{(3)}-\sigma_R^{(3)}$. The normalized dichroism ($\mathrm{CD_{norm}}$), defined as $(\mathrm{CD_{norm}})=(\sigma_L^{(3)}-\sigma_R^{(3)})/(\sigma_L^{(3)}+\sigma_R^{(3)})$, is also considered by many authors.

The CD can be obtained from our experiment by subtracting the TDCS obtained in the HUP mode from that obtained in the HUN mode at the same relative angle φ_1. This latter condition is required to eliminate the φ_1-dependent second term in Eq. (3). One then obtains

$$\begin{aligned}(\mathrm{CD})&=\frac{1}{|S_3|}(\sigma_{\mathrm{HUN}}^{(3)}-\sigma_{\mathrm{HUP}}^{(3)})\\&=+4\sin\phi_{12}\,\mathrm{Im}(a_g a_u^*)=-4\sin\phi_{12}|a_g||a_u|\sin\chi.\end{aligned} \tag{4}$$

Important properties of the CD emerge from the relation above. The $\sin\phi_{12}$ factor implies that the CD vanishes at $\phi_{12}=0°$ and 180°, when $\vec{k}_1$, $\vec{k}_2$, and $\vec{k}_\gamma$ are coplanar, in

agreement with the original prediction of Berakdar and Klar [39]. The transformation $\phi_{12} \rightarrow 2\pi - \phi_{12}$ leaves the amplitudes a_g and a_u unchanged but changes the sign of the geometrical factor $\sin \phi_{12}$ so that the CD is antisymmetric about $\phi_{12} = \pi$. The CD is also antisymmetric about $R = 1$ (i.e., $R < 1$, $R > 1$), as this corresponds to $\chi \rightarrow \chi \pm \pi$.

In contrast to the raw CD, the normalized CD cannot be determined from our experiment, due to the second term in Eq. (2). The sum of the TDCSs obtained in the two modes actually contains, in addition to the required unpolarized contribution $\sigma_R^{(3)} + \sigma_L^{(3)}$, a residual term proportional to S_1.

One disadvantage of our ''fixed spectrometer'' operating mode is that our measurements are performed for fixed emission directions of the lower-energy electron in the laboratory frame (fixed Φ_1), not in the relative frames (fixed φ_1). However, the TDCSs measured at $\Phi_1 = 145°$ in the HUN mode and at $\Phi_1 = 80°$ in the HUP mode correspond to very close relative angles, namely, $\varphi_1 = 110°$ and 115°, respectively, and they have a common subset of ϕ_{12} values ranging from $\approx 110°$ to 200°. Given the previously discussed uncertainties in λ, it is quite reasonable to use these TDCSs to obtain the CD. Another problem arises from the fact that the integrated flux available cannot be considered constant when one switches from one mode to the other: we have overcome this difficulty by normalizing $\sigma_{\mathrm{HUN}}^{(3)}$ to $\sigma_{\mathrm{HUP}}^{(3)}$ at $\phi_{12} = 180°$ where the CD vanishes according to Eq. (4).

The experimental CD is compared with that predicted by H$\mathcal{R}$M-SOW in Figs. 5(a) and 5(b) for $R = 5$ and 11, respectively. Due to the antisymmetry about $\phi_{12} = 180°$, we shall restrict our discussion to $\phi_{12} < 180°$. The experimental data are normalized to the absolute scale of the H$\mathcal{R}$M-SOW results, and agreement between experiment and theory is very good. For both $R = 5$ and 11, the CD is negative, and its magnitude increases from zero as ϕ_{12} is decreased from 180°, peaks at $\sim 150°$, and then decreases towards zero at smaller mutual angles. The ϕ_{12} dependences of the CD for the two energy-sharing ratios are very similar for the energies E_1, E_2 considered in this paper, implying that the dynamic factor for the two cases is almost constant. It should be also noted that the sign of the present CD is opposite to that of the CD obtained by Mergel *et al.* [46] and Achler *et al.* [47]: this comes from the fact that these authors use the fast electron as the reference electron, whereas we use the slow one.

One can infer an interesting property of the CD from Eq. (4), namely, that it may have ''dynamic nodes'' related to the modulus of the complex amplitudes or to their relative phase, in addition to the ''geometrical nodes'' associated with the $\sin \phi_{12}$ factor. The actual existence of these dynamic nodes was first predicted by Berakdar *et al.* [40], who, using Coulomb waves, showed that for a fixed ϕ_{12} of 90°, a zero in the CD occurs at $R \sim 10.3$ and $E \sim 34$ eV. Some experimental evidence for the existence of these nodes has appeared recently [45,47]. The $\mathrm{CD}_{\mathrm{norm}}$ values measured by Achler *et al.* [47] at 20 eV excess energy for $R = 0.026$, 0.14, and 0.38 all decrease from clearly positive values at $\phi_{12} \sim 135°$ to negative values at the smallest ϕ_{12} value investigated, which is $\sim 80°$, thus passing through zero at some intermediate mutual angle. A symmetric zero should then be observed in the symmetric range of ϕ_{12} values, i.e., between 225° and 280°. This is not the case, however, as the experimental data are not perfectly antisymmetric. Although this weakens the experimental evidence for the existence of dynamic nodes, they are nevertheless clearly supported by the CCC calculations [24]. The present study, at 60 eV excess energy for $R = 5$ or 11, gives no evidence for dynamic nodes. The H$\mathcal{R}$M-SOW theory predicts no such nodes whatever the value of ϕ_{12}, and this is confirmed by our experiment in the restricted range of ϕ_{12} values that are accessible. This situation makes these dynamic nodes appear as an interesting topic for further study, since they appear to occur only at certain values of E,R, and ϕ_{12}, and are likely to be extremely sensitive to the approximations in the theoretical approaches. Furthermore, the (E,R,ϕ_{12}) ''position'' of these nodes is relatively straightforward to measure.

V. CONCLUSIONS

In this paper we have presented TDCSs at 60 eV above threshold for $R = 5$ and 11, measured using elliptically-polarized radiation over a wide range of emission angles of the two electrons. These nonabsolute experimental TDCSs, and the deduced CD, have been found to be in good agreement with those determined by the H$\mathcal{R}$M-SOW theory. No dynamic nodes are found in either the experimental (within the explored ϕ_{12} range) or theoretical CD for this excess energy and these R values. Predictions of the R,E, and ϕ_{12} conditions for dynamic nodes, using a variety of theoretical methods, will provide an interesting challenge for future experimental studies.

ACKNOWLEDGMENTS

This work was predominantly funded by EPSRC. S.C. acknowledges the Leverhulme Trust for support. We thank Dr. Miyauchi and Dr. Sekine, and Professor Koide for their independent polarimeter measurement of the tilt angles during the beam time period. We also express our thanks to all those at the Photon Factory who made this work possible.

[1] J. S. Briggs and V. Schmidt, J. Phys. B **33**, R1 (2000).
[2] O. Schwarzkopf, B. Krässig, J. Elmiger, and V. Schmidt, Phys. Rev. Lett. **70**, 3008 (1993).
[3] O. Schwarzkopf, B. Krässig, and V. Schmidt, J. Phys. IV **3**, 169 (1993).
[4] A. Huetz, P. Lablanquie, L. Andrić, P. Selles, and J. Mazeau, J. Phys. B **27**, L13 (1994).
[5] O. Schwarzkopf, B. Krässig, V. Schmidt, F. Maulbetsch, and J. S. Briggs, J. Phys. B **27**, L347 (1994).
[6] P. Lablanquie, J. Mazeau, L. Andrić, P. Selles, and A. Huetz, Phys. Rev. Lett. **74**, 2192 (1995).
[7] G. Dawber, L. Avaldi, A. G. McConkey, H. Rojas, M. A. Mac-

Donald, and G. C. King, J. Phys. B **28**, L271 (1995).
[8] O. Schwarzkopf and V. Schmidt, J. Phys. B **28**, 2847 (1995); **29**, 1877 (1996).
[9] J. Mazeau, L. Andrić, A. Jean, P. Lablanquie, P. Selles, and A. Huetz, in *Atomic and Molecular Photoionization*, edited by A. Yagishita and T. Sasaki (Universal Academy, Tokyo, 1996), pp. 31–38.
[10] J. Viefhaus, L. Avaldi, F. Heiser, R. Hentges, O. Gessner, A. Rüdel, M. Wiedenhöft, K. Wieliczek, and U. Becker, J. Phys. B **29**, L729 (1996).
[11] R. Dörner, H. Bräuning, J. M. Feagin, V. Mergel, O. Jagutzki, L. Spielberger, T. Vogt, H. Khemliche, M. H. Prior, J. Ullrich, C. L. Cocke, and H. Schmidt-Böcking, Phys. Rev. A **57**, 1074 (1998).
[12] J. P. Wightman, S. Cvejanović, and T. J. Reddish, J. Phys. B **31**, 1753 (1998).
[13] H. Bräuning, R. Dörner, C. L. Cocke, B. Krässig, A. S. Kheifets, I. Bray, A. Bräuning-Demain, K. Carnes, S. Dreuil, V. Mergel, P. Richard, J. Ullrich, and H. Schmidt-Böcking, J. Phys. B **31**, 5149 (1998).
[14] S. Cvejanović, J. P. Wightman, T. J. Reddish, F. Maulbetsch, M. A. MacDonald, A. S. Kheifets, and I. Bray, J. Phys. B **33**, 265 (2000).
[15] A. Huetz and J. Mazeau, Phys. Rev. Lett. **85**, 530 (2000).
[16] S. A. Collins, A. Huetz, T. J. Reddish, D. P. Seccombe, and K. Soejima, Phys. Rev. A **64**, 062706 (2001).
[17] P. Bolognesi, R. Camilloni, M. Coreno, G. Turri, J. Berakdar, A. S. Kheifets, and L. Avaldi, J. Phys. B **34**, 3193 (2001).
[18] C. Dawson, S. Cvejanović, D. P. Seccombe, T. J. Reddish, F. Maulbetsch, A. Huetz, J. Mazeau, and A. S. Kheifets, J. Phys. B **34**, L525 (2001).
[19] G. Turri, L. Avaldi, P. Bolognesi, R. Camilloni, M. Coreno, G. Stefani, J. Berakdar, and A. S. Kheifets, Phys. Rev. A **65**, 034702 (2002).
[20] M. Brauner, J. S. Briggs, and H. Klar, J. Phys. B **22**, 2265 (1989); F. Maulbetsch and J. S. Briggs, *ibid.* **26**, 1679 (1993); J. Berakdar and J. S. Briggs, Phys. Rev. Lett. **72**, 3799 (1994).
[21] A. K. Kazansky and V. N. Ostrovsky, J. Phys. B **27**, 447 (1994); **27**, 5197 (1994).
[22] D. Proulx and R. Shakeshaft, Phys. Rev. A **48**, R875 (1993); M. Pont and R. Shakeshaft, J. Phys. B **28**, L571 (1995); M. Pont, R. Shakeshaft, F. Maulbetsch, and J. S. Briggs, Phys. Rev. A **53**, 3671 (1996).
[23] I. Bray and A. T. Stelbovics, Phys. Rev. A **46**, 6995 (1992); A. S. Kheifets and I. Bray, J. Phys. B **31**, L447 (1998).
[24] A. S. Kheifets and I. Bray, Phys. Rev. Lett. **81**, 4588 (1998).
[25] T. N. Rescigno, M. Baertschy, W. A. Isaacs, and C. W. McCurdy, Science **286**, 2474 (1999); M. Baertschy, T. N. Rescigno, W. A. Isaacs, X. Li, and C. W. McCurdy, Phys. Rev. A **63**, 022712 (2001).
[26] M. S. Pindzola and F. Robicheaux, Phys. Rev. A **57**, 318 (1998).
[27] J. Colgan, M. S. Pindzola, and F. Robicheaux, J. Phys. B **34**, L457 (2001).
[28] L. Malegat, P. Selles, and A. Kazansky, Phys. Rev. A **60**, 3667 (1999).
[29] L. Malegat, P. Selles, and A. K. Kazansky, Phys. Rev. Lett. **85**, 4450 (2000).
[30] P. Selles, L. Malegat, and A. K. Kazansky, Phys. Rev. A **65**, 032711 (2002).
[31] A. Huetz, P. Selles, D. Waymel, and J. Mazeau, J. Phys. B **24**, 1917 (1991).
[32] B. Krässig, in *Correlations, Polarization and Ionization in Atomic Systems*, edited by D.H. Madison and M. Schulz, AIP Conf. Proc. No. 604 (AIP, Melville, NY, 2002), pp. 12–17.
[33] L. Malegat, F. Citrini, P. Selles, and P. Archirel, J. Phys. B **33**, 2409 (2000).
[34] L. Malegat, P. Selles, and A. Huetz, J. Phys. B **30**, 251 (1997).
[35] L. Malegat, P. Selles, P. Lablanquie, J. Mazeau, and A. Huetz, J. Phys. B **30**, 263 (1997).
[36] K. Soejima, A. Danjo, K. Okuno, and A. Yagishita, Phys. Rev. Lett. **83**, 1546 (1999).
[37] S. Cvejanović and T. J. Reddish, J. Phys. B **33**, 4691 (2000).
[38] A. S. Kheifets and I. Bray, Phys. Rev. A **65**, 022708 (2002).
[39] J. Berakdar and H. Klar, Phys. Rev. Lett. **69**, 1175 (1992).
[40] J. Berakdar, H. Klar, A. Huetz, and P. Selles, J. Phys. B **26**, 1463 (1993).
[41] J. Berakdar, J. Phys. B **31**, 3167 (1998).
[42] J. Berakdar, J. Phys. B **32**, L27 (1999).
[43] A. Kheifets, I. Bray, K. Soejima, A. Danjo, K. Okuno, and A. Yagishita, J. Phys. B **32**, L501 (1999).
[44] J. Berakdar and H. Klar, Phys. Rep. **340**, 474 (2001); J. Berakdar, Czech. J. Phys. (to be published).
[45] J. Viefhaus, L. Avaldi, G. Snell, M. Wiedenhöft, R. Hentges, A. Rüdel, F. Schäfers, D. Menke, U. Heinzmann, A. Engelns, J. Berakdar, H. Klar, and U. Becker, Phys. Rev. Lett. **77**, 3975 (1996).
[46] V. Mergel, M. Achler, R. Dörner, Kh. Khayyat, T. Kambara, Y. Awaya, V. Zoran, B. Nyström, L. Spielberger, J. H. McGuire, J. Feagin, J. Berakdar, Y. Azuma, and H. Schmidt-Böcking, Phys. Rev. Lett. **80**, 5301 (1998).
[47] M. Achler, V. Mergel, L. Spielberger, R. Dörner, Y. Azuma, and H. Schmidt-Böcking, J. Phys. B **34**, 965 (2001).
[48] J. A. R. Samson, W. C. Stolte, Z. X. He, J. N. Cutler, Y. Lu, and R. J. Bartlett, Phys. Rev. A **57**, 1906 (1998).
[49] S. Yamamoto, T. Shioya, S. Sasaki, and H. Kitamura, Rev. Sci. Instrum. **60**, 1834 (1989).
[50] Insertion Device Handbook, edited by H. Kitamura KEK Report No. 89-24, Tsukuba (1990).
[51] Y. Kagoshima, S. Muto, T. Miyahara, T. Koide, S. Yamamoto, and H. Kitamura, Rev. Sci. Instrum. **63**, 1289 (1992).
[52] H. Kimura, T. Miyahara, J. Gota, K. Mayama, M. Yanagihara, and M. Yamamoto, Rev. Sci. Instrum. **52**, 1920 (1995).
[53] T. J. Reddish, G. Richmond, G. W. Bagley, J. P. Wightman, and S. Cvejanović, Rev. Sci. Instrum. **68**, 2685 (1997).
[54] B. Kämmerling and V. Schmidt, J. Phys. B **26**, 1141 (1993).
[55] R. Wehlitz, B. Langer, N. Berrah, S. B. Whitfield, J. Viefhaus, and U. Becker, J. Phys. B **26**, L783 (1993).
[56] S. J. Schaphorst, B. Krässig, O. Schwarzkopf, N. Scherer, V. Schmidt, P. Lablanquie, L. Andric, J. Mazeau, and A. Huetz, J. Electron Spectrosc. Relat. Phenom. **76**, 229 (1995).